Kim, H.W. and Duraisamy, K. and Brown, R.E. (2008) *Aeroacoustics of a coaxial rotor in level flight.* In: 64th American Helicopter Society Annual Forum, Montreal, Canada.

http://eprints.gla.ac.uk/5004/

Deposited on: 11 March 2009

Aeroacoustics of a Coaxial Rotor in Level Flight

Hyo Won Kim*
Visiting Researcher

Karthikeyan Duraisamy
Lecturer

Richard Brown
Mechan Chair of Engineering

Rotorcraft Aeromechanics Laboratory
Department of Aerospace Engineering
University of Glasgow
Glasgow G12 8QQ
United Kingdom

Abstract

The aeroacoustic characteristics of a coaxial system with teetering rotors in level forward flight are compared to those of an equivalent articulated single rotor with the same solidity. A lifting line representation of the blade aerodynamics is coupled to Brown's Vorticity Transport Model to simulate the aerodynamics of the rotor systems. The acoustic field is determined using the Ffowcs Williams-Hawkings equation. Acoustic analysis shows that the principal contribution to noise radiated by both the coaxial and equivalent single rotor systems is at the fundamental blade passage frequency, but that the coaxial rotor generates higher sound pressure levels (by 10 dB for the evaluated configurations) than the equivalent single rotor at all flight speeds. The sources of blade vortex interaction (BVI) noise are investigated and the principal BVI events are identified. For the coaxial rotor, the most intense impulsive noise is seen to be generated by the inter-rotor BVI on the advancing side of the lower rotor. The impulsive noise that is generated by blade vortex interactions for the equivalent single rotor reduces in amplitude as the strength of BVI events on the rotor decreases with forward speed. Conversely, the BVI noise of the coaxial rotor intensifies with increasing flight speed due to the increasing strength of the interaction between the wake of the upper rotor and the blades of the lower rotor. The impulsive noise due to BVI for the coaxial rotor is found to be higher by 20–35 dB compared to the equivalent single rotor. The overall and impulsive noise characteristics of the coaxial system are found to be weakly sensitive to changes in rotor separation and the relative phasing of the rotors.

Nomenclature

Symbols:

C_P	rotor power coefficient
C_T	rotor thrust coefficient
F	force vector
M	Mach number
R	rotor radius
a_0	speed of sound
p_L	acoustic pressure
r	observer distance from source
t	time
μ	advance ratio
τ	acoustic source time
ψ	blade azimuth

Abbreviations:

BVI	blade vortex interaction
SPL	sound pressure level (dB)
OASPL	overall SPL (dB)
BVISPL	blade vortex interaction SPL (mid frequency 5–40/rev) (dB)

Important note: throughout this paper, the lower rotor of the coaxial system should be taken to rotate anticlockwise, and the upper rotor to rotate clockwise, when viewed from above. In single rotor simulations, the rotor should be taken to rotate anticlockwise when viewed from above.

---
* Postgraduate Research Student, Imperial College London, United Kingdom

Introduction

A recent resurgence of interest in the coaxial rotor configuration has been prompted by its potential to meet modern requirements for helicopters with increased speed and load carrying capabilities. The obvious advantage of a coaxial rotor over a conventional main rotor-tail rotor configuration is the

elimination of the need for a tail rotor as the required torque balance is achieved inherently within the contra-rotating main rotor system. This appealing advantage of contra-rotating twin coaxial rotors prompted some of the early rotorcraft pioneers to exploit the configuration, yet, the single main rotor-tail rotor configuration remains the prevailing platform for most military and civil helicopters.

There has been a significant research interest in the characteristics of coaxial rotor aerodynamics in several countries including Russia, the US, the UK and Japan (see Ref. 1). Unfortunately, most of the existing literature has failed to provide a truly fair comparison of the relative performance of conventional and coaxial rotors. A recent study has argued that the fairest comparison between conventional and coaxial rotors is on the basis of equal solidity, and identical overall blade number and aerodynamic properties. On this basis the coaxial rotor is shown to consume less power, mainly due to its slightly lower consumption of induced power compared to the equivalent single rotor (Ref. 2). The advantage of the coaxial rotor system in terms of reduced power requirement was shown to be enhanced by the introduction of significant flapwise stiffness (Ref. 3). Additionally, compared to single rotor systems, coaxial rotors with significant flapwise stiffness can operate at lower tip speeds than the equivalent articulated system, thus offering the potential to postpone the detrimental effects of compressibility on aerodynamic and acoustic performance to higher forward speeds (Ref. 4).

While the aerodynamic characteristics of coaxial rotors are not as well studied as those of conventional rotors, detailed investigations of the acoustic performance of coaxial rotors are even more rare in the open literature. In the early 1980s Peterson and Mosher (Ref. 4) conducted a full scale wind tunnel experiment on Sikorsky's XH-59A rotor. In this test, acoustic measurements were obtained over a range of rotor lift coefficients, advance ratios and shaft angles. The conclusions from this study were that the noise level of the coaxial system increases with loading on the rotor and as the shaft angle approaches zero just as observed in the case of a typical single rotor. The microphone array used in the experiment was too sparse to reveal any detail of the acoustics radiation pattern that was generated by the rotor but some anomalies in the measured data were attributed to impulsive effects. Blade vortex interaction (BVI) noise was speculated to be influenced by the distribution of lift between the upper and lower rotors but unfortunately, within the scope of the experiment, no firm conclusions could be drawn on the effect of interactions between the upper and lower rotors and their consequences for the resulting acoustic char-

acteristics of the coaxial system. More recently, Boyd *et al.* (Ref. 5) provided a numerical comparison between the acoustic signature of a Bö105 model rotor that was similar to the rotor used in the HART II experiments described in Ref. 6, and a fictitious coaxial system, consisting of two Bö105 rotors contra-rotating about the same axis. The wakes of the rotors were approximated by a system of single tip vortices. In this comparison, it was found that the coaxial system generated higher BVI noise compared to the single rotor system. It was also observed that the interference effects between the upper and lower rotors of a coaxial system had a significant effect on its resulting acoustic character. Based on comparisons against experimental results from the HART II rotor test (Ref. 6), it was concluded, however, that a vortex filament model may not have been accurate enough to represent the wake to the detail required for accurate acoustic predictions.

Aeroacoustics is a rapidly maturing discipline and its application to helicopter rotors is a very active field of research (refer to Ref. 7 for a review of recent accomplishments). Coaxial rotor systems generally do not seem to have been subject to detailed aeroacoustic study, however. The aim of this paper is to compare the aeroacoustic characteristics of a coaxial rotor system with those of an aerodynamically equivalent, conventional single rotor. Since a significant part of the lower rotor of the coaxial system operates in the wake of the upper rotor, additional noise associated with the inter-rotor BVIs (which do not occur on a single rotor) can be expected, and a detailed study of these interactions and the associated noise produced by a coaxial rotor operating in forward flight is presented.

Computational Model

Aerodynamics

The Vorticity Transport Model (VTM) developed by Brown (Ref. 8) and extended by Brown and Line (Ref. 9) is used for the aerodynamic computations presented in this paper. In the VTM, a Weissinger-L version of lifting line theory is used (along with a look-up table for the two-dimensional aerodynamic characteristics of the rotor blade sections) to represent the blade aerodynamics in conjunction with an Eulerian representation of the dynamics of the vorticity in the rotor wake. The convection algorithm implemented in the VTM is particularly effective in controlling the local rate of numerical dissipation of vorticity, allowing the integrity of vortical structures in the rotor wake to be preserved for many rotor revolutions. The use of an adaptive grid system in a semi-Lagrangian manner to track the evolving vorticity field enhances

the computational efficiency of the method. The overall cell count is reduced by using a sequence of nested grids in which increasingly coarser cells are arranged with increasing distance from the rotor. In this respect, the VTM is thus particularly well suited to resolving the wake-induced interactions between the twin main rotors in the coaxial configuration, and hence the sources of acoustic radiation within the system.

Acoustics

The acoustic field of the rotor system is determined using the Ffowcs Williams-Hawkings equation (Ref. 10). The instantaneous acoustic pressure, $p_L(t)$, at a given observer location due to a discrete point force F moving at Mach number M, is given by

$$p_L(t) = \frac{1}{4\pi a_0} \left[\frac{\partial}{\partial t} \left(\frac{F_r}{r(1-M_r)} \right) + \frac{a_0 F_r}{r^2(1-M_r)} \right]_\tau \tag{1}$$

where a_0 is the speed of sound, r is the distance between the observer and the source, $F_r = F \cdot r$, and $M_r = M \cdot r$. The term in the square bracket is evaluated at the source time τ at which the sound was emitted. The integral in Eq. 1 is implemented numerically using the Farassat-1A formulation in which the source time derivatives are transformed to observer time derivatives (Refs. 7, 11). Since the blade surface in the aerodynamic model is represented by a series of panels, the force contributed by each panel is treated as a point source located at the collocation point of the panel. The noise produced by these sources is then propagated according to Eq. 1. The aerodynamic effects of the thickness of the blade are introduced through a look-up table of airfoil characteristics, but the lifting line model within the VTM otherwise assumes an infinitesimally thin blade. The thickness noise is thus modelled independently using a source-sink pair attached to each panel along the length of the blades (Ref. 12). Noise due to quadrupole terms is neglected in the present work. The coupled VTM-acoustics methodology has been used previously to predict the acoustics of the HART II rotor (Ref. 13), where good agreement between the computed pressure time histories and sound pressure levels was demonstrated against measured data for three representative flight conditions involving strong BVIs.

Rotor Configuration

Model Geometry

The rotor configuration used in this study mimics that used by Harrington (referred to as 'rotor 1' in Ref. 14), consisting of two identical articulated two-bladed rotors that contra-rotate about the same axis. The rotor blades are untwisted and have symmetrical NACA four-digit airfoil sections. While the blade planform has a linear taper, the thickness along the span of the blade changes in a non-linear fashion. The span of the rotor blade from the centre of rotation to the tip is 3.81m and the overall solidity of the coaxial rotor is $\sigma = 0.054$. The upper and lower rotors are separated vertically by 19% of the rotor radius.

Unlike in the original experiments described in Refs. 14 and 15 (and also in Ref. 5), where comparisons of the performance of the coaxial rotor were made against one of its own constituting rotors, in this work, aerodynamic and acoustic comparisons are made against a suitably defined single rotor with equal solidity and the same blade geometry as the coaxial rotor. This allows for an acoustic comparison between two systems in which the rotor blades operate within a comparable aerodynamic environment. Thus, bearing in mind that the coaxial rotor consists of two two-bladed rotors, the equivalent single rotor consists of four co-planar blades. To match the original experimental setup, the hubs of the coaxial rotor are modelled to have a teetering configuration while the equivalent single rotor is given a fully articulated hub. It should be noted that the loading distribution on coaxial rotors with articulated hubs, and hence their acoustic behaviour, can be significantly different to that when rotor has some degree of hub stiffness. The effects of hub stiffness on the acoustic properties of the coaxial system are not considered in this paper, however.

Trim Method

The trim algorithm implemented in the VTM is a first-order dynamical system where the rate of change of the control inputs are driven by the difference between prescribed target values of the rotor forces and moments and their instantaneous values. A more detailed account of the trim model can be found in Ref. 3. In all cases considered in the present study, the coaxial rotor system is trimmed to zero net moment in yaw using differential collective pitch input to the upper and lower rotors whilst satisfying a pre-specified thrust requirement. The cyclic pitch inputs to the upper and lower rotor are coupled so that both rotors receive the same control inputs. The coupled cyclic input is used to tilt the thrust vector forward in order to generate a propulsive force while maintaining zero lateral force on the system. Although the fuselage is not explicitly modelled, the effect of the fuselage on the propulsive force required from the rotor is represented by the drag of a flat plate with an area
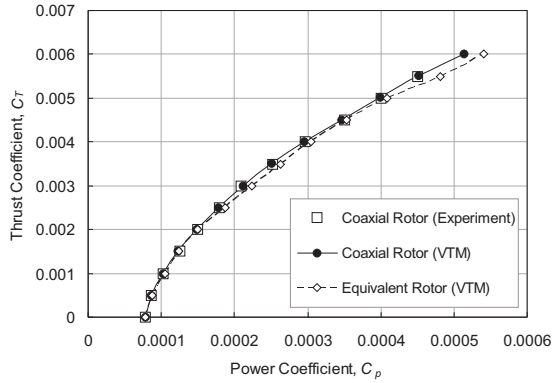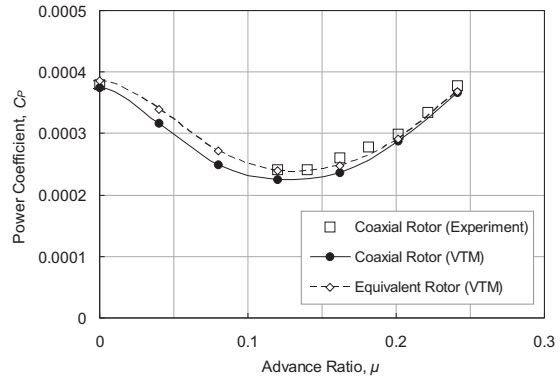
(a) Hover, $M_{tip} = 0.45$ (b) Steady forward Flight, $C_T = 0.0048$, $M_{tip} = 0.42$

Figure 1: *Comparison of predicted power consumption of coaxial rotor against experimental measurements in hover and forward flight.*

of 2% of the rotor disc area to follow the approach that was adopted in Dingeldein's experiment.

The equivalent single rotor is trimmed to the same overall forces and moments as the coaxial rotor system at the same forward speed thus yielding a fair comparison between the performance of the two systems.

Aerodynamic Verification

The experimental measurements of the power consumption of Harrington's 'rotor 1' in hover (Ref. 14) and in forward flight (Ref. 15) provide a valuable set of data against which to assess the ability of the VTM to predict the aerodynamic performance of coaxial rotors.

Figure 1 shows a comparison between this data and the power consumption of the coaxial rotor as predicted by the VTM. The predictions of the VTM correlate well with the experimental results in both hover and forward flight. While the trend within the experimental data is well captured, the power requirement of the coaxial rotor in forward flight is slightly under-predicted by the VTM.

Figure 1 also compares the power consumption of the coaxial and equivalent single rotor systems and shows that the coaxial rotor consumes slightly less power than the equivalent single rotor in almost all flight conditions. The reduction in power is most pronounced at high thrust in hover and at low forward flight speeds. The majority of the power saving on the coaxial rotor originates from a reduction in the induced component of power that comes about through the subtle redistribution of loading on the rotor disc that results from localised interactions between the upper and lower rotors (Ref. 2).

The observed agreement between the predicted performance of the coaxial rotor system against this well-regarded set of experimental data lends confidence in the ability of the VTM to provide the acoustic model with a reliable loading pattern on the rotors from which the sound radiation from the system can be computed with some confidence.

Acoustic Analysis

Detailed analysis of the acoustic characteristics of the coaxial rotor and the equivalent single rotor in forward flight is limited to two representative flight speeds (advance ratios of $\mu = 0.12$ and 0.24) in order simply to contrast the differences in the behaviour of the system at low and high advance ratios. Figure 2 shows the structure of the respective wakes in forward flight at these advance ratios. The gross features of the far wakes of both configurations are superficially very similar at the low advance ratio: both wakes clearly show the helicoidal individual blade vortices to roll up to form a pair of large 'super-vortices' some distance downstream of the rotor disc. There are, however, interactional aerodynamic features in the coaxial system that are not found on the conventional rotor. In particular, the complex manner in which the tip vortices from the upper and lower rotors interweave in the gap between the two rotors leads to a complicated pattern of inter-rotor BVIs that are obviously not encountered with the conventional system. The tip vortex dynamics during the formation of the super-vortices of the coaxial system is also considerably more complicated than for the conventional rotor — as can be seen, the individual tip vortices from the upper and lower rotors wind around each other, at least at this advance ratio, to form a single pair of super-vortices rather than, as might be imagined, forming two distinct structures, one for each rotor. As shown in Fig. 2(b), this interaction is counteracted to a certain extent at the higher advance ratio by the forward tilt of the rotor. This tilt, together
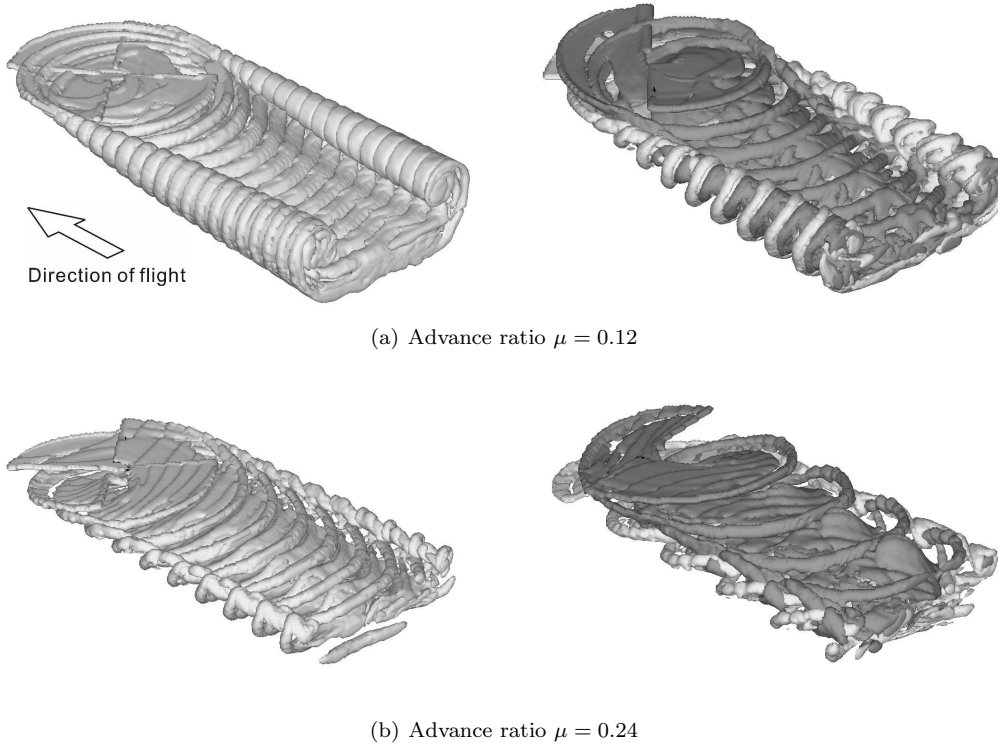
Direction of flight

(a) Advance ratio $\mu = 0.12$

(b) Advance ratio $\mu = 0.24$

Figure 2: *Overall wake structure in forward flight visualised by a surface of constant vorticity. (Left: equivalent single rotor. Right: coaxial rotor. Coaxial rotor: Wake from upper rotor shaded darker than that from the lower rotor.)*

with the increased convection rate of the vorticity in the wake, acts to maintain the separation between the wakes that are produced individually by the upper and lower rotors until significantly further downstream.

Overall Noise Characteristics

Figure 3 shows a contour plot of the overall sound pressure level (OASPL) that is produced on a horizontal observer plane located at a distance of one rotor radius below the hub[1] by the coaxial rotor and its equivalent single rotor at an advance ratio of $\mu = 0.12$. The noise levels are seen to peak at a sequence of 'hot spots' that are located directly underneath the tips of the rotor discs. Figures 4 and 5 show the time history and frequency spectrum, respectively, of the acoustic pressure at the hot spot at the rear edge (at $\psi = 0°$) of each of the rotor systems. As is typical of measured acoustic data from conventional helicopters in both model and flight tests (e.g. Refs. 6 and 16), the major contribution to the noise produced by the equivalent single rotor is at very low frequencies (less than five times the blade passage frequency). At the corresponding locations of maximum noise on

the observer plane, the SPL of the coaxial rotor is found to be around 10 dB higher than that of the equivalent single rotor. This trend appears to persist for all advance ratios between $\mu = 0.12$ and $\mu = 0.24$.

Figure 4 shows that the noise due to the lower rotor of the coaxial system is highly impulsive even at the location of maximum overall noise. Correspondingly, it is evident from Figure 5 that the noise of the coaxial rotor is distributed over a much wider range of frequencies than that produced by the equivalent single rotor. Similarly though to the single rotor, the main contribution to the noise produced by the coaxial rotor is at low frequency. It is worth noting that the low frequency noise is related to the low harmonic airloads on the rotor blades. Impulsive noise that is radiated to the ground, on the other hand, is primarily caused by wake interactions. In a coaxial rotor system, interactions between the wake produced by the upper rotor and the blades of the lower rotor act as an additional source of noise that is not present in a single rotor system. Given the focus of this paper on the acoustics of coaxial rotor systems, further discussion will concentrate on the high frequency noise that is associated with these BVIs.
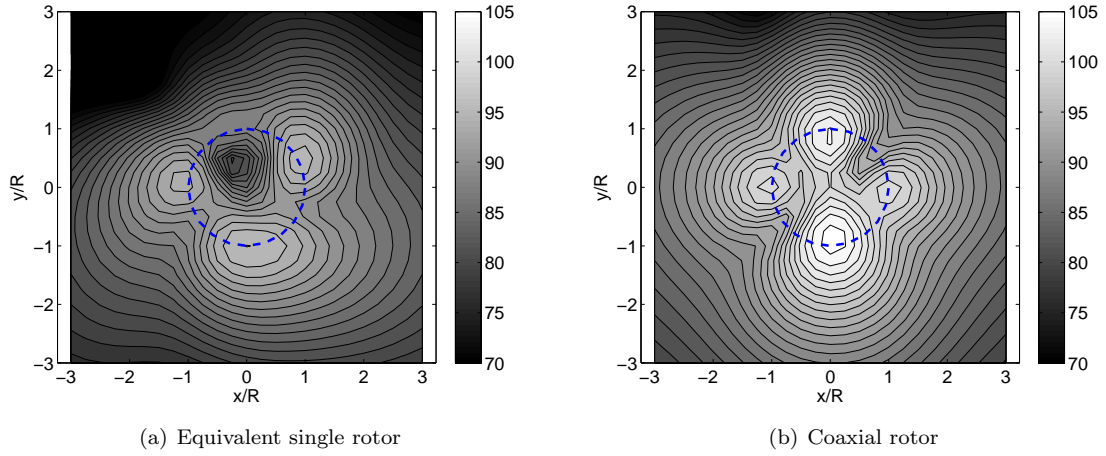
---

[1]For the coaxial system, the observer plane is located one rotor radius below the hub of the lower rotor.

(a) Equivalent single rotor

(b) Coaxial rotor

Figure 3: *Overall SPL in decibels in forward flight at $\mu = 0.12$. (Direction of flight along positive y-axis.)*
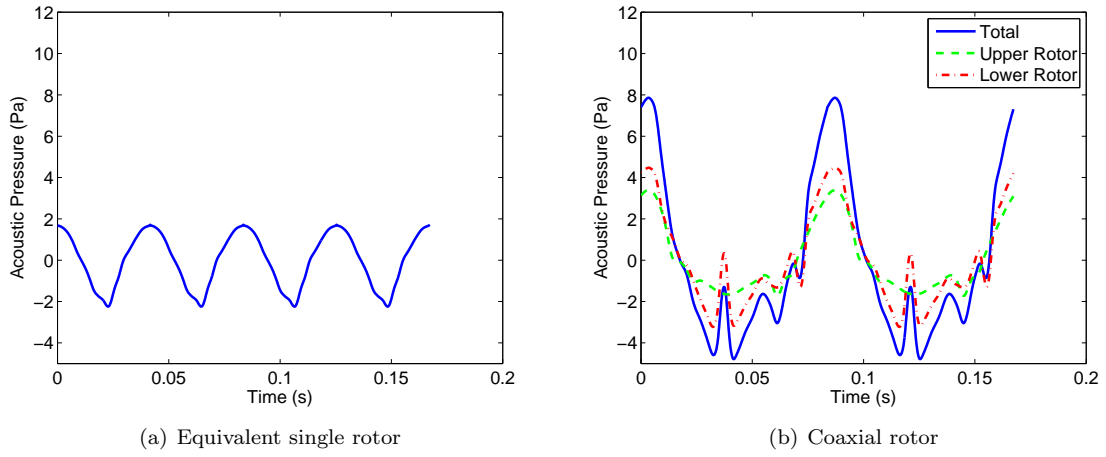

(a) Equivalent single rotor

(b) Coaxial rotor

Figure 4: *A time history of acoustic pressure over one rotor revolution one rotor radius below the tip of the rotor disc at $\psi = 0°$ for $\mu = 0.12$.*
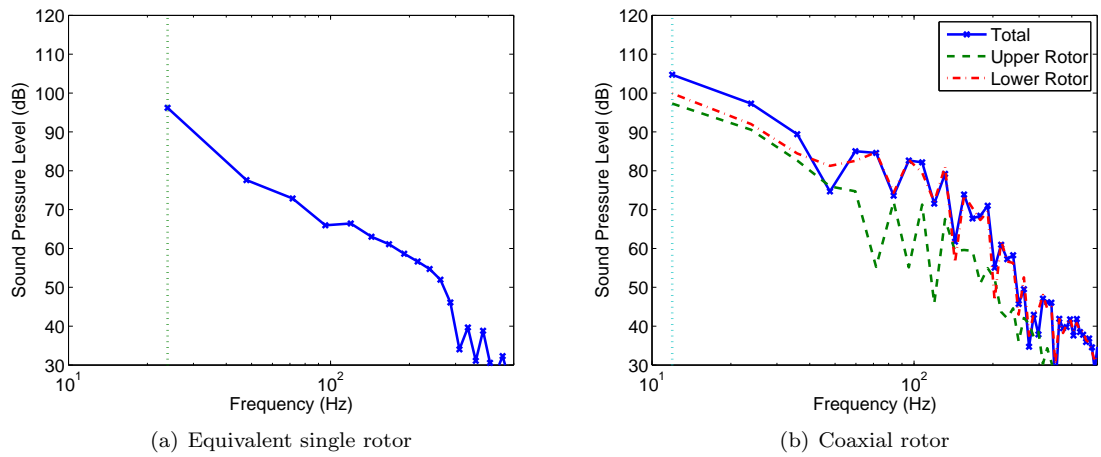

(a) Equivalent single rotor

(b) Coaxial rotor

Figure 5: *Frequency spectrum of the sound pressure level one rotor radius below the tip of the rotor disc at $\psi = 0°$ for $\mu = 0.12$. The vertical dotted line represents the fundamental blade passage frequency.*
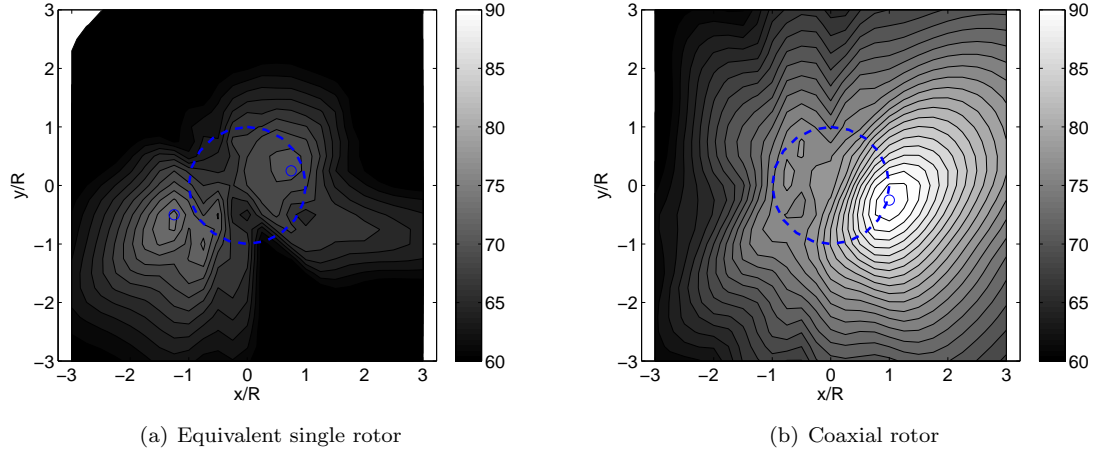
(a) Equivalent single rotor

(b) Coaxial rotor

Figure 6: *BVI sound pressure levels (5–40/rev) (in dB) at $\mu = 0.12$.*

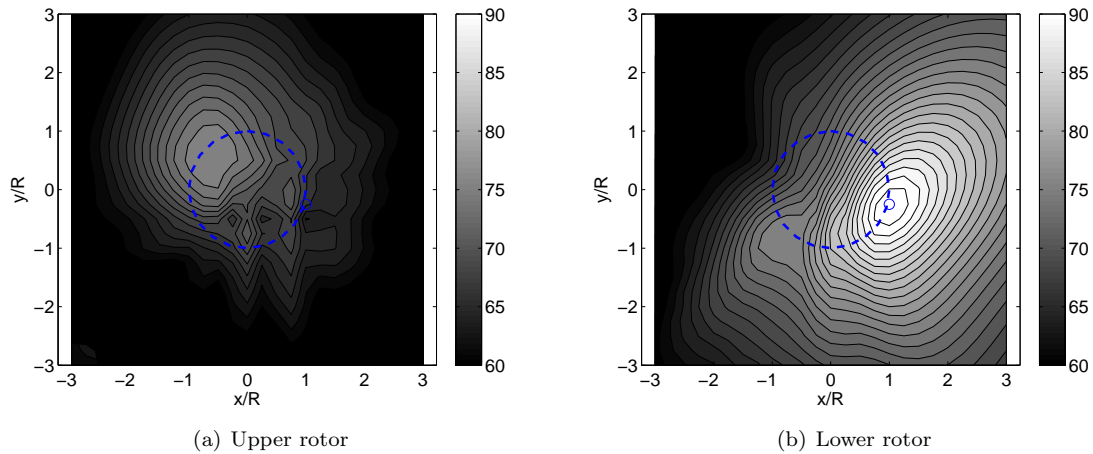(a) Upper rotor

(b) Lower rotor

Figure 7: *BVI sound pressure levels (5–40/rev) in decibels for individual rotors in coaxial configuration at $\mu = 0.12$.*

BVI Noise Characteristics

The contour plots presented in Fig. 6 (and also in Fig. 11) contrast the distribution of SPL on the observer plane in the BVI frequency range (computed by aggregating the acoustic energy in the Fourier modes ranging from 5/rev to 40/rev) for the equivalent single rotor and coaxial rotor.

For the equivalent single rotor at an advance ratio $\mu = 0.12$ (Figure 6(a)), two BVI hot spots are evident on the observer plane. One of these is situated directly below the advancing side of the rotor and the other below the retreating side. Such a radiation pattern is typical of a single rotor in forward flight (Refs. 6, 13). It is well recognised that the dipole nature of the loading noise results in a propagation of sound that is directed primarily downwards (Ref. 16). The hot spots are thus positioned roughly beneath the corresponding positions on the rotor where the BVI sources are most intense, that is, where the combination of miss-distance and alignment of the passing vortices results in the strongest impulsive loads on the rotor blades.

For the coaxial rotor (Figure 6(b)), the highest sound pressure is concentrated under the advancing side of the lower rotor. The sound pressure level at the hot spot (marked by a circle in the Figure) is appreciably higher (by 16 dB) than the highest sound pressure level generated by the equivalent single rotor (Figure 6(a)) at this flight condition.

Figure 7 shows the separate contributions from the upper and lower rotors to the noise generated by the coaxial rotor. The figure shows the lower rotor to be the dominant source of noise on the observer plane below the rotor, as might be expected from the additional wake interactions to which the lower rotor is subjected. This inference is supported by Figure 8 in which the time history of the acoustic pressure at the hot spot on the advancing side of the lower rotor is shown over one rotor revolution. The two highly impulsive peaks in the acoustic pressure correspond to identical events on each of the two blades of the lower rotor of the coaxial system. The origin of these impulses can be understood by considering the distribution of the acoustic sources on the blade over a single rev-
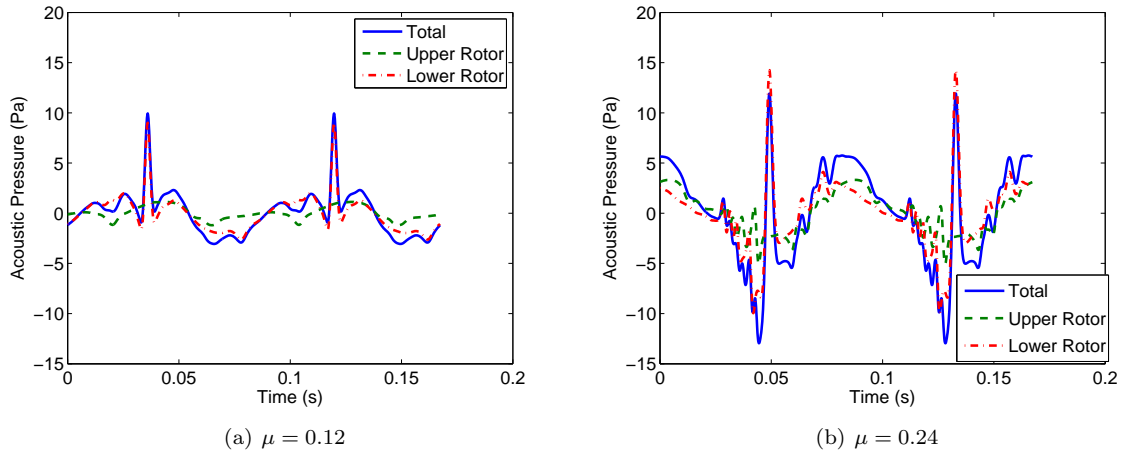
(a) $\mu = 0.12$ (b) $\mu = 0.24$

Figure 8: *Time history of acoustic pressure at the BVI hot spot (see Figure 6) for coaxial rotor.*

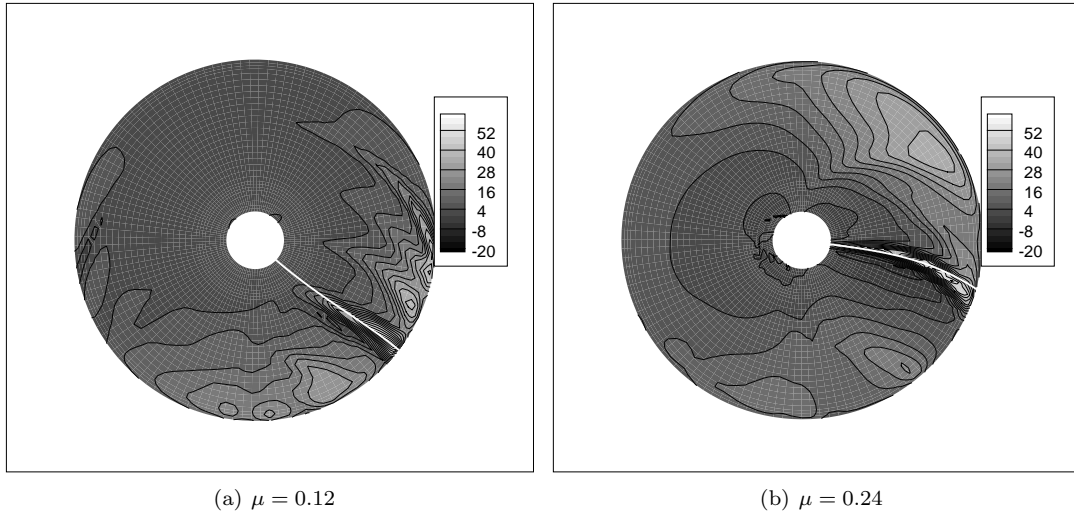(a) $\mu = 0.12$ (b) $\mu = 0.24$

Figure 9: *Acoustic source density (loading noise, Pa/m^2) on lower rotor of coaxial system as evaluated at the BVI hot spot. Also shown (as a white line) is the locus of sources corresponding to time $t = 0.036s$ in (a) and $t = 0.049s$ in (b)*

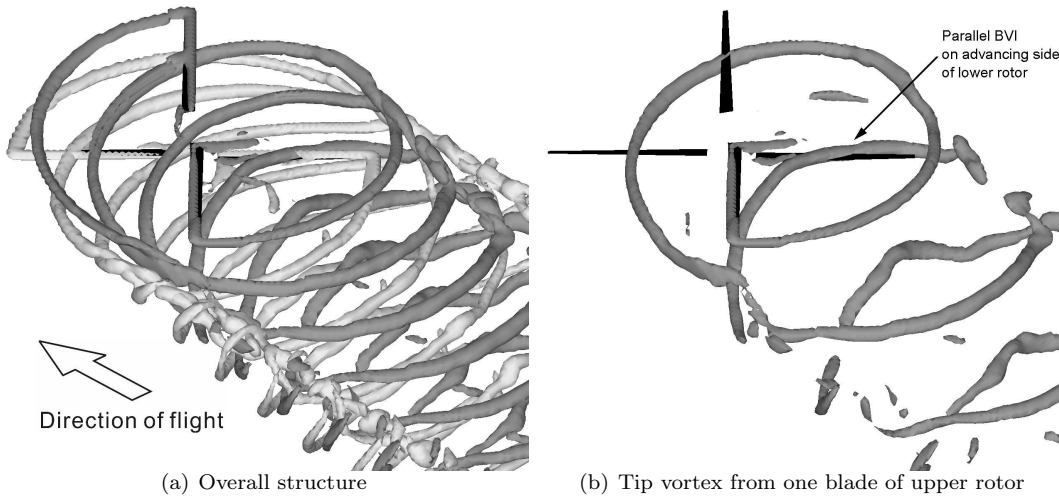(a) Overall structure   (b) Tip vortex from one blade of upper rotor

Figure 10: *Tip vortex structure of coaxial rotor at $\mu = 0.12$ showing inter-rotor BVI via parallel impingement.*

(a) Equivalent single rotor
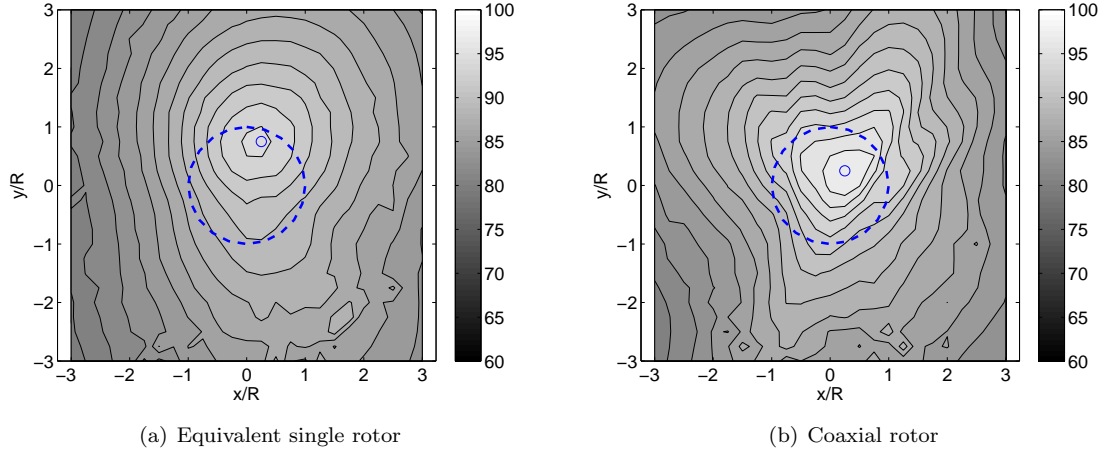
(b) Coaxial rotor

Figure 11: *BVI sound pressure levels (5–40/rev) in decibels at $\mu = 0.24$.*

olution of the lower rotor. Figure 9(a) shows the density of the noise sources due to loading (evaluated from the loading noise term in Eq. 1 and scaled by the local panel area) in 'source time' *i.e.* corresponding to the location of the blade when the sound was generated. It should be noted that the distribution of source density will of course differ for each observer location. The plot is thus generated from the perspective of an observer located at the BVI hot spot below the advancing side of the lower rotor. Furthermore, the plot is constructed from the sources located on only one of the blades. Also indicated in Figure 9(a) (as a thick white line) is the locus of all the sources that contribute to the noise at the specific observer time (at $t = 0.036$s in Figure 8(a)) corresponding to the peak in impulsive noise. It is evident that the intense interaction at the azimuthal location of $\psi \approx 45°$ (corresponding to the locus of sources contributing to the noise at $t = 0.036$s) is responsible for the impulsive noise. Figure 10(a) shows the overall structure of the wake at the instant at which one of the blades of the lower rotor is at an azimuth of $\psi = 45°$. In Fig. 10(b) some of the detail of this plot is suppressed to show the specific inter-rotor BVI that is responsible for the impulsive noise. It is evident that during this BVI, the blade on the lower rotor passes directly through the axis of a trailing vortex from the upper rotor. Furthermore, the trailing vortex is essentially parallel to the blade span at the time of impingement, thus generating a highly impulsive incident velocity field over a significant portion of the blade span.

At higher advance ratio ($\mu = 0.24$), the character of the BVI acoustic pattern generated by the equivalent single rotor is somewhat different to that observed at lower advance ratio. The hot spot under the advancing side shifts towards the front of the rotor disc (to approximately $\psi = 170°$ as shown
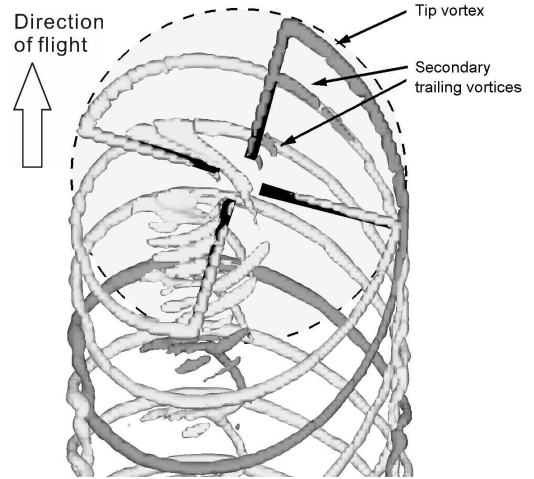

Figure 12: *A rotor blade of the equivalent single rotor at $\mu = 0.24$ interacting with tip vortex from preceding blade at $\psi \approx 170°$. Trailed vorticity generated by this blade is shaded dark to highlight secondary trailing vorticity generated by this interaction.*

in Figure 11). The primary origin of the noise at this hot spot is an oblique blade vortex interaction as shown in Figure 12. Even though the BVI is not parallel, the prolonged interaction (from $\psi \approx 90°$ to $270°$) generates high intensity noise. Interestingly, the figure also shows secondary trailing vortices that are generated as a result of the abrupt changes in loading along the span of the blade that are induced by the BVIs. The pattern of BVIs on the rotor disc at this advance ratio is somewhat sparser than at lower advance ratio. Indeed, the increasing forward tilt of the rotor disc with forward speed that is required to provide the propulsive component of force on the system increases the miss-distance between the wake vortices and
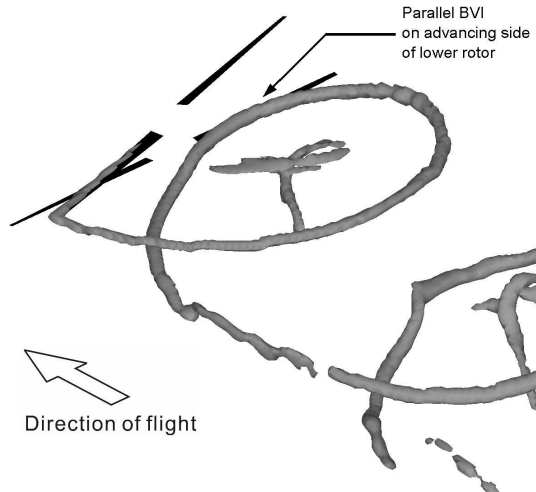
Figure 13: *Tip vortex structure from the upper rotor of the coaxial system impinging on an advancing lower rotor blade showing parallel inter-rotor BVI at $\mu = 0.24$.*

the blades and thus acts to weaken the strength of individual BVI events.

On the other hand, the BVI induced sound pressure level on the observer plane for the coaxial rotor has the same qualitative pattern at high advance ratio as observed at lower forward flight speed. The location of the hot spot moves further inboard as shown in Figure 11(b), but the highly impulsive peaks in the time history of the acoustic pressure seen for $\mu = 0.12$ persist at $\mu = 0.24$ (see Fig. 8). The amplitude of the peaks in the acoustic pressure at high forward speed are significantly larger and occur slightly later than at low forward speed, however. The high intensity BVI that is evident at an observer time of $t = 0.049$s corresponds to the source time indicated by the white line (at roughly $\psi = 80°$) on the plot of decomposed noise sources due to loading shown in Figure 9(b). The impulsive noise field appears to be dominated by a BVI event that occurs as one of the rotor blades approaches the azimuth at which it experiences maximum incident velocity. Figure 13 captures the wake structure at instant at which one of the blades of the lower rotor is at an azimuth of $\psi = 80°$. The figure shows the blade to be interacting strongly with a tip vortex that is generated from the upper rotor. As at lower forward speed, the axis of the interacting vortex lies almost parallel to the blade, resulting in a highly impulsive change in loading along its span and significant acoustic radiation.

Even though the intensity of the BVIs on the equivalent single rotor reduces with forward speed, the BVI sound pressure level on the observer plane one radius below the rotor is significantly higher for *both* rotors at $\mu = 0.24$ than at $\mu = 0.12$. This seeming anomaly in the case of the equivalent rotor

is a result of the dominance of the near field contribution to the loading noise (the second term in Eq. 1). Furthermore, the noise from the equivalent single rotor is less impulsive when compared to the coaxial rotor.

Far-Field Noise

In the following discussion, sound pressure levels on a hemispherical observer surface of radius $2R$, centered at the rotor hub (in the case of the coaxial rotor, at the hub of the lower rotor) are considered. This representation of the acoustic field generated by the rotor is useful for purposes of interpreting far-field acoustics as the surface can roughly be considered as a hemispherical source of sound with the same acoustic properties as the rotor at its centre. Figure 14(a) shows the maximum SPL (OASPL) on the hemisphere at three forward flight speeds. For both the coaxial system and the equivalent single rotor, the rate of increase of the OASPL with flight speed is roughly similar although the coaxial rotor is consistently noisier by approximately 8 dB.

For the equivalent single rotor, the contribution of the BVISPL to the overall SPL increases significantly as the advance ratio is increased from $\mu = 0.12$ to 0.16 as shown in Figure 14(a). On the other hand, Figure 14(b) shows the loading-induced component of noise in the BVI range to reduce with increasing flight speed. This trend arises from the increased disc tilt that is required to generate the propulsive force at higher speeds as described earlier. The increase in the impulsive noise in the BVI range of frequencies in Figure 14(a) for the equivalent single rotor is thus due to intensification of thickness noise at higher flight speeds.

As explained in the previous section, for the coaxial system, the inter-rotor BVIs are intensified as the forward speed is increased. Indeed, Figure 14(b) shows a rapid increase in the loading noise within the BVI frequency range as flight speed is increased. Figure 15 shows the associated contours of SPL mapped on to the hemispherical observer surface at various forward speeds for the coaxial rotor. Note that in this case, the hemispherical surface extends above the level of the lower rotor hub by $0.2R$ to capture the in-plane propagation of noise from this rotor as the forward speed is increased. The directivity of the far-field noise, as observed in this figure, shifts towards the front of the rotor. This is because of the primary BVI occurring at a later azimuth as the speed of flight is increased. A similar trend in directivity of impulsive far-field noise, though at a reduced SPL, was observed for the equivalent single rotor.
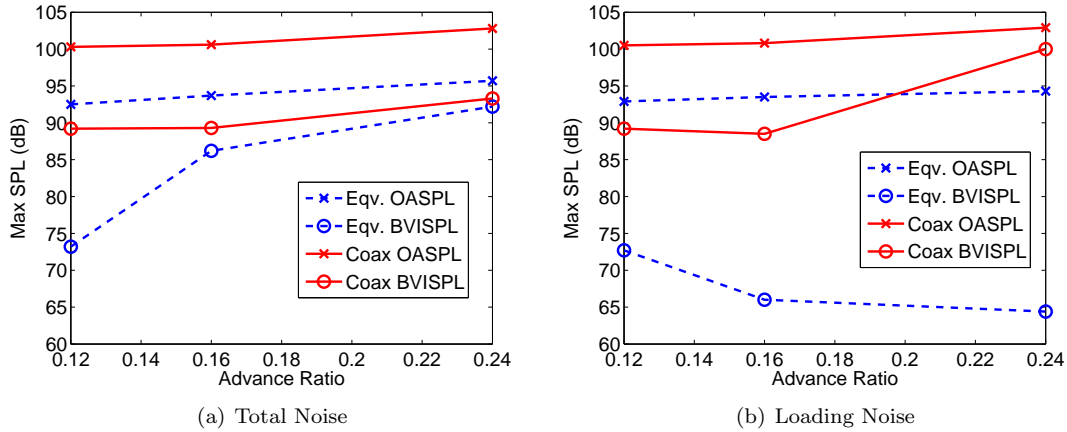
(a) Total Noise

(b) Loading Noise

Figure 14: *Maximum OASPL and BVISPL in decibels at $M_{tip} = 0.42$ on a hemispherical observer surface of radius $2R$, centered on the rotor hub.*

Implications of Minor Design Changes

Since BVI noise propagates in the direction of the ground, the high BVI noise levels generated by the coaxial system in comparison to the equivalent single rotor may work against the certification and routine use of coaxial rotor helicopters. For the configuration evaluated in this work, the intense impulsive noise that is generated by the coaxial rotor has been shown to be primarily due to the inter-rotor blade vortex interaction on the advancing side of the lower rotor. There is, however, a certain amount of design flexibility inherent in the coaxial system for instance, rotor separation and blade phasing, that may be optimised to alter this interaction, with the aim of alleviating impulsive noise. In order to gain a nominal assessment of the sensitivity of the noise radiated by the coaxial system to such design changes, two representative configurational modifications to the original coaxial system were performed:

First, a change of blade phasing was considered. The original configuration was such that the blades of the top and bottom rotors were aligned with each other at azimuthal angles of $0°, 90°, 180°$ and $270°$. This phasing was altered, such that blade over-passage was shifted to $45°, 135°, 225°$ and $315°$.

Second, an increase in rotor separation was considered. The vertical separation between the top and bottom rotors was set to $0.247R$, amounting to an increase of 30% compared to that of the original configuration.

Figure 16 shows the effect of these design changes on the BVI sound pressure levels (at $\mu = 0.12$) on a horizontal plane one rotor radius below the hub of the lower rotor. This figure should be compared to Fig. 6(b). The change in rotor phasing does not affect the maximum sound pressure levels and ap-

pears simply to shift the location of the BVI hot spot. This is an important result since it suggests that the intensity of BVI noise produced by the coaxial system may not be sensitive to rotor phasing. Although the results are not shown here, the overall noise levels were also found to be unaffected by rotor phasing. The four OASPL hot spots, however, were found to be $45°$ out of phase with those shown in Figure 3(b). The increased rotor separation causes a decrease of 2 dB in the maximum BVI sound pressure level. The weight, drag and structural dynamic penalties of the elongated mast may not be justified for such a marginal reduction in noise levels.

Conclusions

In this study, the aeroacoustic characteristics of a coaxial rotor in forward flight is compared to those of a suitably defined aerodynamically equivalent single rotor.

In the intermediate far-field (less than two rotor radii from the rotor disc), the main contribution to the noise generated by both the coaxial and the equivalent single rotor systems is at the fundamental blade passage frequency. The coaxial rotor examined is this study is consistently noisier than the equivalent single rotor by approximately 10 dB. As expected, the noise generated by the coaxial rotor examined in this study is highly impulsive, principally as a result of blade-wake interactions on the lower rotor.
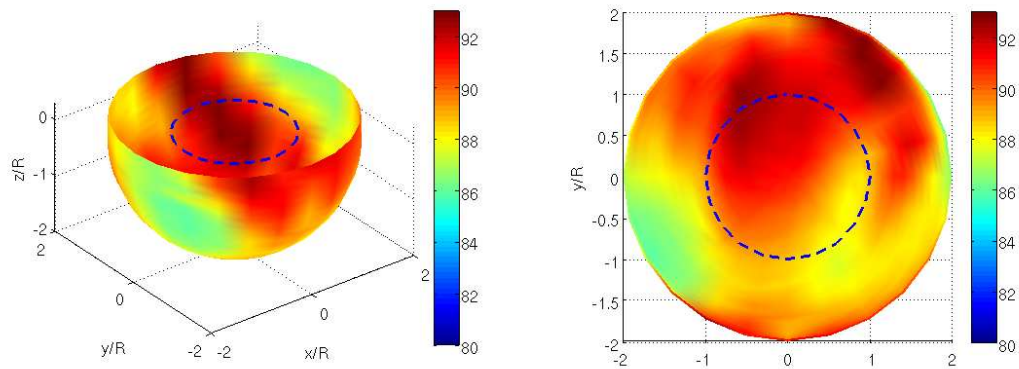
The BVI loading noise for the equivalent single rotor reduces with increasing forward speed as the disc tilt required to provide the propulsive force component to the system increases the miss distance between blades and vortices and reduces the strength of individual BVI events. The BVI noise of the coaxial rotor is intensified due to the increas-
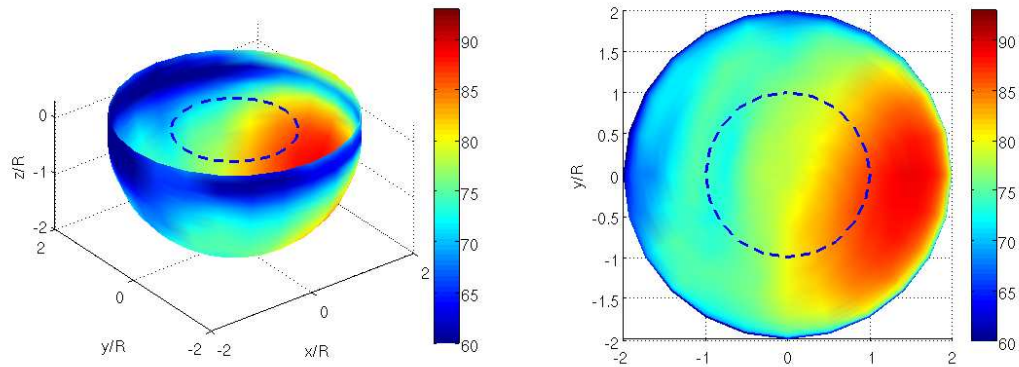
(a) $\mu = 0.12$
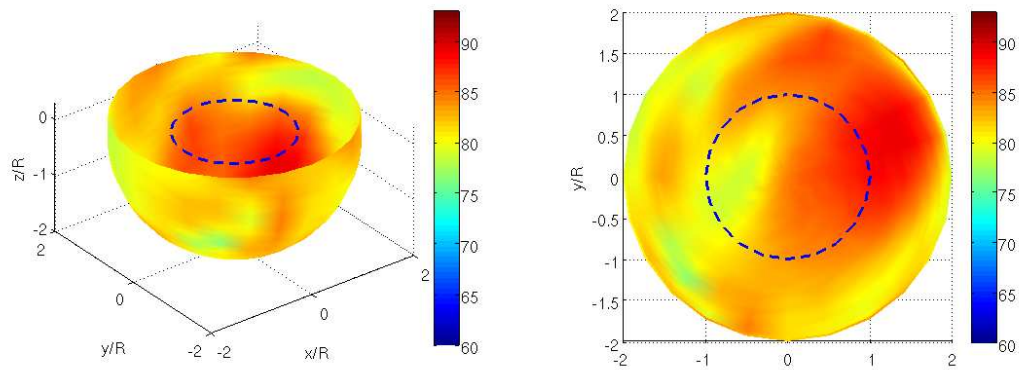
(b) $\mu = 0.16$

(c) $\mu = 0.24$

Figure 15: *BVISPL in decibels for coaxial rotor on a hemispherical surface of radius $2R$ centered on the hub of the lower rotor. (Left: isometric view. Right: top view.)*
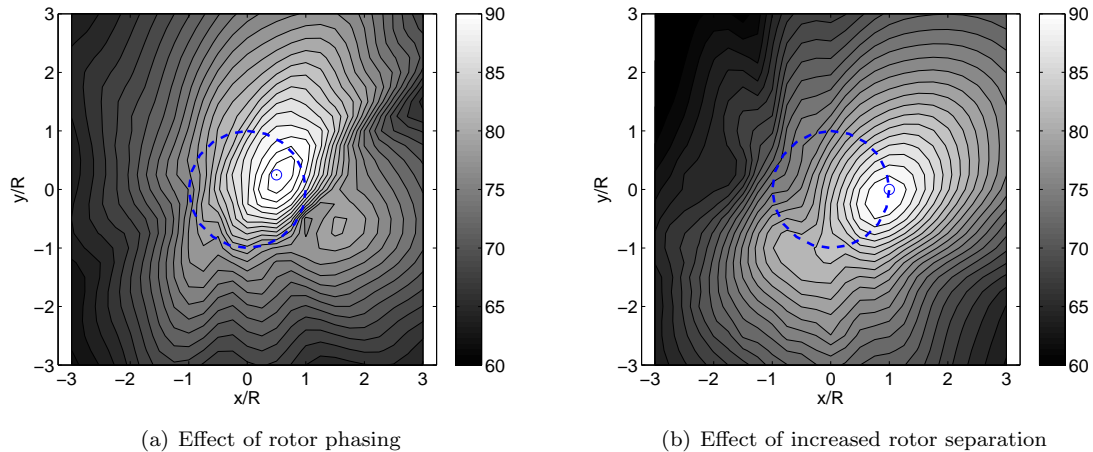
(a) Effect of rotor phasing

(b) Effect of increased rotor separation

Figure 16: *BVI sound pressure levels (5–40/rev) (in dB) for coaxial rotor with design changes at $\mu = 0.12$.*

ing strength of the interaction between a tip vortex from the upper rotor and the advancing blade of the lower rotor with increasing forward speed. The impulsive noise due to BVI on a hemispherical surface that is located two rotor radii from the rotor hub is about 20–35 dB higher for the coaxial rotor than for the equivalent single rotor, depending on the forward speed of the rotor.

The higher BVI noise of coaxial rotor helicopters, may ultimately hinder routine use in civilian and military applications, but it may be possible to optimise the design of the rotor to mitigate the noise levels.

A change of blade phasing between the upper and lower rotors had a marginal effect on the noise characteristics of the coaxial system. An increase of 30% in the separation distance between the upper and lower rotors similarly resulted in a marginal decrease in overall and BVI noise, suggesting the relative insensitivity of the configuration to such strategies.

References

[1]Coleman, C.P., "A Survey of Theoretical and Experimental Coaxial Rotor Aerodynamic Research," NASA TP-3675, March 1997.

[2]Kim, H.W., Brown, R.E., "Coaxial Rotor Performance and Wake Dynamics in Steady and Manoeuvring Flight," *American Helicopter Society 62nd Annual Forum*, Phoenix, AZ, 9–11 May 2006.

[3]Kim, H.W., Brown, R.E., "Impact of Trim Strategy and Rotor Stiffness on Coaxial Rotor Performance," *1st AHS/KSASS International Forum on Rotorcraft Multidisciplinary Technology*, Seoul, Korea, 15–17 October 2007.

[4]Peterson, R.L., Mosher, M., "Acoustic Measurements of a Full-Scale, Coaxial, Hingeless Rotor Helicopter," NASA TM-84349, June 1983.

[5]Boyd, Jr., D.D., Burley, C.L., Conner, D.A., "Acoustic Predictions of Manned and Unmanned Rotorcraft Using the Comprehensive Analytical Rotorcraft Model for Acoustics (CARMA) Code System," *American Helicopter Society International Specialists' Meeting on Unmanned Rotorcraft*, Phoenix, AZ, 18–20 January 2005.

[6]van der Wall, B.G., Junker, B., Burley, C.L., Brooks, T.F., Yu, Y.H., Tung, C., Raffel, M., Richard, H., Wagner, W., Mercker, E., Pengel, K., Holthusen, H., Beaumier, P., Delrieux, Y., "The HART II Test in the LLF of the DNW—a Major Step towards Rotor Wake Understanding," *28th European Rotorcraft Forum*, Bristol, UK, 17–20 September 2002.

[7]Brentner, K., Farassat, F., "Modeling Aerodynamically Generated Sound of Helicopter Rotors," *Progress in Aerospace Sciences*, Vol. 39, 2003.

[8]Brown, R.E., "Rotor Wake Modeling for Flight Dynamic Simulation of Helicopters," *AIAA Journal*, Vol. 38, No. 1, January 2000, pp. 57–63.

[9]Brown, R.E., Line, A.J., "Efficient High-Resolution Wake Modeling Using the Vorticity Transport Equation," *AIAA Journal*, Vol. 43, No. 7, April 2005, pp. 1434–1443.

[10]Ffowcs Williams, J.E., Hawkings, D.L. "Sound Generation by Turbulence and Surfaces in Arbitrary Motion," *Philosophical Transactions of the Royal Society of London. Series A, Mathematical and Physical Sciences*, Vol.264, No.1151, May 1969, pp. 321–342.

[11]Farassat, F., Succi, G.P. "A Review of Propeller Discrete Frequency Noise Prediction Technology with Emphasis on Two Current Methods for Time

Domain Calculations," *Journal of Sound and Vibration*, Vol. 71, No. 3, 1980, pp. 399–419.

[12]Schmitz, F., Yu, Y., "Theoretical Modeling of High-Speed Helicopter Impulsive Noise," *Journal of the American Helicopter Society*, Vol.23, No.1, 1979.

[13]Kelly, M.E., Duraisamy, K., Brown, R.E., "Blade Vortex Interaction and Airload Prediction using the Vorticity Transport Model," *American Helicopter Society Specialists' Conference on Aeromechanics*, San Francisco, CA, 23–25 January 2008.

[14]Harrington, R.D., "Full-Scale-Tunnel Investigation of the Static-Thrust Performance of a Coaxial Helicopter Rotor," NACA TN-2318, March 1951.

[15]Dingeldein, R.C., "Wind-Tunnel Studies of the Performance of Multirotor Configurations," NACA TN-3236, August 1954.

[16]Schmitz, F.H., "Aeroacoustics of Flight Vehicles: Theory and Practice," NASA Reference Publication 1258, Vol. 1, Chapter 2, August 1991, pp. 65–149.